NTNU

Kunnskap for en bedre verden

NTNU

TKJ4200 - Irreversible thermodynamics

Onsager-symmetry in athermal two-phase flow in porous media with the Lattice-Boltzmann model

Authors:
Håkon Pedersen
Christian Ulrichsen

Supervisors:
Professor Signe Kjelstrup
Professor Dick Bedeaux
Dr. Santanu Sinha

Fall 2021

Abstract

We model two-phase flow in a porous medium using a Lattice-Boltzmann simulation of a system generated by CT-scans of rock samples. From this simulation we calculate conductivity coefficients and check for symmetry in the cross-correlated terms. We explore the fundamental theory behind the Onsager reciprocal relations, $L_{ij} = L_{ji}$, and formulate the entropy production and conductivity matrices for the flow of two immiscible fluids in an athermal porous medium. The fluctuation-dissipation theorem is used to derive the expressions used to calculate the conductivity coefficients in the Lattice-Boltzmann model. The Lattice-Boltzmann model and theory are discussed, and connections from the model to physical properties are explained. Preliminary results indicate that, at least under certain conditions, symmetry is obeyed within the estimated uncertainty. Possible reasons for deviation under the conditions where symmetry is not obeyed are discussed.

Contents

List of Figures

List of Tables

Acknowledgements

A huge thank you to professors Signe Kjelstrup and Dick Bedeaux, as well as Dr. Santanu Sinha, for all of their support. Their patient and thorough responses to our questions, and their insightful suggestions for paths to explore helped make this project a truly rewarding experience. We are very grateful for all of their time and expertise.

1 Introduction

Coupled transport plays a major role in nature. With non-equilibrium thermodynamics, we can formulate and understand this property in systematically. It is the basis for a number of applications, such as the thermocouple, thermoelectric generators, and electricity generation from reverse electrodialysis. Microscopic reversibility and symmetry of the coupled transport coefficients simplify calculations and help to improve our understanding of these systems. One area where these are not as well understood is in fluid flows in porous media [25]. Flows in porous media play a key role in the oil and gas industry, but they are also critical in all kinds of electrochemical processes for storage and power important to developing sustainable industry and combating climate change, such as underground storage of hydrogen and the sequestration of carbon dioxide in porous materials [9, 22]. These fall directly in line with the United Nations' sustainability goals such as sustainable industrialization, affordable and clean energy, and climate action [23].

An earlier publication by Winkler et al. modeled two-phase flow in a network model of a porous medium in order to demonstrate coupled transport coefficient symmetry, or Onsager reciprocal relations, and their results indicate that these reciprocal relations exist for their system [25]. Their process involved building a two-dimensional (2-D) network model of a representative elementary volume (REV) for their system, and then measuring the flow of two immiscible fluids through it. One of the central goals of this project is to use a different model to produce results that we can then compare to theirs. As such, we closely follow their process for calculating the coupled transport coefficients, as well as emulating the conditions for their simulation as best we can. Our aim is to build a comparable three-dimensional (3-D) model of an REV from CT-scans of rock samples, and then run a Lattice-Boltzmann simulation of the flow of two immiscible fluids through that model. We also explore Onsager reciprocal relations from a more general sense, to develop a better understanding of the theory and assumptions that give rise to that symmetry as well as how they relate to the two-phase flow system.

2 Theory and model

2.1 Onsager's proof of reciprocal relations

When Lars Onsager published his proof of the reciprocal relations in 1931, he made two key assumptions. The first assumption is that of microscopic reversibility. This is the idea that even if a process is on the whole irreversible, microscopic steps on very short time scales behave reversibly. The second assumption is that microscopic changes in fluctuations follow the same linear relation as their macroscopic counterparts [17, 18, 11].

Microscopic reversibility begins with a basic set of extensive thermodynamic variables A_i, and their fluctuations α_i. It is important that these variables are symmetric with respect to time reversal, which means that fluctuations in these variables are reversed when time is reversed. The internal energy of a system left isolated for a length of time sufficient to establish equilibrium is an example of this kind of variable. Examples of these kinds of fluctuations are defined by:

$$\alpha_i = A_i - \langle A_i \rangle \tag{1}$$

Here, the fluctuations α_i are defined as the difference between the thermodynamic variable A_i and its mean, $\langle A_i \rangle$. These fluctuations are key for microscopic reversibility, which tells us that the chance of seeing fluctuation α_i at time t, followed by α_j at time $(t+\tau)$, is *on average* the same as seeing α_j at time t followed by α_i at time $(t+\tau)$:

$$\langle \alpha_i(t)\alpha_j(t+\tau) \rangle \;=\; \langle \alpha_j(t)\alpha_i(t+\tau) \rangle \tag{2}$$

The next assumption to define is that of the linear relation of microscopic fluctuations. Starting

with the macroscopic definition of fluxes, J_i, being linear functions of the forces, X_j, and their conductivities, L_{ij}:

$$J_i = \sum_{j=1}^{n} L_{ij} X_j \tag{3}$$

From this relation we draw the linear relation of microscopic fluxes, $J_i(t)$, and forces, $X_j(t)$:

$$J_i(t) = \sum_{j=1}^{n} L_{ij} X_j(t) \tag{4}$$

Once these assumptions have been made, the rest of the proof can be carried out.

A system's entropy is at it's maximum when the system is in equilibrium. So the entropy of a system, S, given some maximum entropy, S_{eq}, can be written as:

$$S = S_{eq} + \Delta S(\alpha_1, \ldots, \alpha_n) = S_{eq} - \frac{1}{2} \sum_{j,i=1}^{n} g_{ji} \alpha_j \alpha_i + \ldots \tag{5}$$

Here, S_{eq}, being a maximum value, is a constant. The ΔS term is then the difference (deviation) between the current entropy and the maximum, with ΔS being a function of fluctuations $\alpha_1 \ldots \alpha_n$. These changes are not necessarily linear, as the Taylor expansion results in the linear order terms equaling zero. This ΔS term is then expanded in equation (5) using a Taylor expansion, producing a tensor value g_{ji} defined by:

$$g_{ji} = \left(-\frac{\partial^2 \Delta S}{\partial \alpha_j \partial \alpha_i} \right)_{\alpha_1 = \cdots = \alpha_n = 0} \tag{6}$$

This tensor term is a symmetric matrix, and thus a factor of $\frac{1}{2}$ is needed to compensate for a double appearance of each combination of independent variables α_i and α_j. Higher orders of the expansion would give more complicated tensor terms, but their contributions are usually small. Next we introduce the normalized probability density for the fluctuations:

$$f(\alpha_1, \ldots, \alpha_n) = \frac{e^{\Delta S / k_B}}{\int_{-\infty}^{\infty} d\alpha_1 \ldots d\alpha_n e^{\Delta S / k_B}} \tag{7}$$

Where k_B is the Boltzmann constant. This function f takes a set of fluctuations α_i and returns the probability of seeing that set. The function is normalized such that an integration of f across all possible α_i is equal to one. Being a normalization, the denominator is a constant and the whole can be rewritten as:

$$f(\alpha_1, \ldots, \alpha_n) = \frac{e^{\Delta S / k_B}}{N_\alpha} \tag{8}$$

where N_α is the normalization constant. Definitions of the thermodynamic fluxes and forces from equations (3) and (4) are important for relating the conductivities to the entropy and Boltzmann distribution. Onsager defined the force, X_i, of a system as follows:

$$X_i = \frac{\partial S}{\partial A_i} = \frac{\partial \Delta S}{\partial \alpha_i} \tag{9}$$

describing how entropy drives the relaxation of the system back to equilibrium. Taking our definition of the force in equation (9) and relating it to our expansion of the entropy in equation (5) we can see that:

$$X_i = \frac{\partial \Delta S}{\partial \alpha_i} = \frac{\partial}{\partial \alpha_i}\left(-\frac{1}{2}\sum_{j,i=1}^{n} g_{ji}\alpha_j\alpha_i + \dots\right) = -\sum_{j=1}^{n} g_{ji}\alpha_j + \dots \tag{10}$$

The conjugate flux of the force X_i is defined as follows:

$$J_i(t) = \frac{dA_i(t)}{dt} = \frac{d\alpha_i(t)}{dt} \tag{11}$$

describing the movement of thermodynamic variable A_i as the system moves towards equilibrium. An important conclusion from these definitions is that the entropy production of the system is defined by the products of these fluxes and forces. Equations (8) and (9) are combined to produce the following term, the derivation of which is in appendix C:

$$X_i = \frac{k_B}{f}\frac{\partial f}{\partial \alpha_i} \tag{12}$$

Determining the expectation value, or ensemble average, of the product $\alpha_i X_j$, also derived in appendix C, produces:

$$\langle \alpha_i X_j \rangle = -k_B \delta_{ij} \tag{13}$$

Where δ_{ij} is the Kronecker delta, meaning that it is 1 if $i = j$ and 0 otherwise. A Taylor expansion of $\alpha_i(t+\tau)$ around t is then performed:

$$\alpha_i(t+\tau) = \alpha_i(t) + ((t+\tau) - t)\frac{d\alpha_i(t)}{dt} + \dots$$
$$\alpha_i(t+\tau) = \alpha_i(t) + \tau\frac{d\alpha_i(t)}{dt} + \dots$$

And taking this expansion to the linear order, and using the relation in equation (11) and substituting equation (4), the result is the following:

$$\alpha_i(t+\tau) = \alpha_i(t) + \tau\sum_{j=1}^{n} L_{ij}X_j(t) \tag{14}$$

With all of these definitions and derivations completed, Onsager's reciprocal relations can be derived. We begin by introducing equation (14) to both sides of equation (2):

$$\begin{aligned}
\langle \alpha_i(t)\alpha_j(t+\tau)\rangle &= \langle \alpha_j(t)\alpha_i(t+\tau)\rangle \\
\left\langle \alpha_i(t)(\alpha_j(t) + \tau\sum_{i=1}^{n} L_{ji}X_i(t))\right\rangle &= \left\langle \alpha_j(t)(\alpha_i(t) + \tau\sum_{j=1}^{n} L_{ij}X_j(t))\right\rangle \\
\left\langle \alpha_i\tau\sum_{i=1}^{n} L_{ji}X_i(t)\right\rangle &= \left\langle \alpha_j\tau\sum_{j=1}^{n} L_{ij}X_j(t)\right\rangle
\end{aligned}$$

And then using equation (13), we know that all products where $i \neq j$ are 0, and we get the expression:

$$\langle \alpha_i L_{ji} X_i(t) \rangle = \langle \alpha_j L_{ij} X_j(t) \rangle$$

And since L_{ij} and L_{ji} are constants, they can be pulled from the average expression to get:

$$\begin{aligned} L_{ji} \langle \alpha_i X_i(t) \rangle &= L_{ij} \langle \alpha_j X_j(t) \rangle \\ L_{ji}(-k_B) &= L_{ij}(-k_B) \end{aligned}$$

And thus we have the relation:

$$L_{ij} = L_{ji} \tag{15}$$

With that, we have an overview of the general proof for the Onsager reciprocal relations. We are interested in determining whether this relation holds for a system with two-phase flow through a porous medium. In other words, do the thermodynamic variables we are looking at obey microscopic reversibility, and does our assumption of the linear relation of microscopic changes in fluctuations hold true? To check this, we will need to start by defining our system and determining expressions for the the entropy production and the conductivity matrix.

2.2 Entropy production

Because the we are looking at the coupling of fluxes, our system must be of a sufficient size that these interactions can be observed. To satisfy this requirement, we will take our system to be a *representative elementary volume*, or REV. This is discussed in detail in section 3.2. Because we are operating in an REV, we use coarse-grained variables for the derivation of the entropy production, rather than pore-scale variables. Our system will consist of two immiscible fluids which are weakly compressible (see section 2.7) flowing through a porous medium. One of these fluids interacts more favorably with the medium; we will call this fluid the wetting fluid, and the other fluid the non-wetting fluid. We assume that there is no electrical potential gradient, and that no reactions occur. We can then introduce our balance equations:

$$\begin{aligned} \frac{\partial \rho_i}{\partial t} &= -\frac{\partial J_i}{\partial x} \\ \frac{\partial u}{\partial t} &= -\frac{\partial J_q}{\partial x} \end{aligned} \tag{16}$$

In these equations, ρ_i is the mass density of either the wetting or the non-wetting fluid, J_i is the mass flux of that fluid, u is the internal energy density, and J_q is the energy flux. The energy flux can be broken down into the measurable heat flux, J_q', the partial molar enthalpy, H_i, and the mass flux. We also formulate our entropy balance equation:

$$\frac{\partial s}{\partial t} = -\frac{\partial J_s}{\partial x} + \sigma \tag{17}$$

Here, s is the entropy density, J_s is entropy flux, and σ is the entropy production. As we did for each of the coupled transport systems introduced in the non-equilibrium thermodynamics course, we will use the local Gibbs equation, under the assumption of microscopic reversibility, in order to find expressions for J_s and σ:

$$\frac{\partial s}{\partial t} = \frac{1}{T}\frac{\partial u}{\partial t} - \frac{1}{T}\sum_{i=1}^{n} \mu_i \frac{\partial \rho_i}{\partial t} \tag{18}$$

where T is temperature and μ_i is the chemical potential of fluid i. When equations (16), (17), and (18) are combined, and terms specific to our system are used, we obtain an expression for the entropy production:

$$\sigma = J_w \left(-\frac{1}{T} \left(\frac{\partial \mu_w^c}{\partial x} + V_w \frac{\partial p}{\partial x} \right) \right) + J_n \left(-\frac{1}{T} \left(\frac{\partial \mu_n^c}{\partial x} + V_n \frac{\partial p}{\partial x} \right) \right) \tag{19}$$

Here, J_i is the mass flux , V_i the volume, and μ_i^c the chemical potential at constant temperature and pressure of fluid i, where subscripts w and n refer to the wetting and non-wetting fluids, respectively. In addition, $\frac{\partial p}{\partial x}$ is the pressure gradient in the system. For the full derivation, see appendix D. From this entropy production expression we can then create our conductivity matrix:

$$\begin{aligned} J_w &= L_{ww} \left(-\frac{1}{T} \left(\frac{\partial \mu_w^c}{\partial x} + V_w \frac{\partial p}{\partial x} \right) \right) + L_{wn} \left(-\frac{1}{T} \left(\frac{\partial \mu_n^c}{\partial x} + V_n \frac{\partial p}{\partial x} \right) \right) \\ J_n &= L_{nw} \left(-\frac{1}{T} \left(\frac{\partial \mu_w^c}{\partial x} + V_w \frac{\partial p}{\partial x} \right) \right) + L_{nn} \left(-\frac{1}{T} \left(\frac{\partial \mu_n^c}{\partial x} + V_n \frac{\partial p}{\partial x} \right) \right) \end{aligned} \tag{20}$$

where L_{ww} and L_{nn} are self-correlated conductivity coefficients, and L_{wn} and L_{nw} are cross-correlated conductivity coefficients. As mentioned in section 2.1, the entropy production of the system is defined by the combination of fluxes and forces. We also know from the second law of thermodynamics that the entropy production is always positive, so that:

$$\sigma = \sum_i J_i X_i \geq 0 \tag{21}$$

If we substitute equation (3) into this expression, we get:

$$\sigma = \sum_i X_i \sum_j L_{ij} X_j = \sum_{i,j} X_i L_{ij} X_j \geq 0 \tag{22}$$

From this, we can see that a system with a single force has a self-correlated conductivity coefficient that must be positive:

$$L_{ii} \geq 0 \tag{23}$$

In addition, *in a system with symmetric cross-correlated conductivity coefficients*, the following is also a consequence of the second law of thermodynamics [11]:

$$L_{ii} L_{ij} - L_{ij} L_{ji} \geq 0 \tag{24}$$

In order to check whether the Onsager reciprocal relations hold for our system, we need to find some way to measure the conductivity coefficients of our system. In addition, we are interested in making sure that the results from our model match the relationship in equation (23), and potentially even equation (24). However, while our model includes values for things like volume and pressure, calculating these coefficients is problematic from this approach. Instead, we will make use of the fluctuation dissipation theorem, and implement it in the same way as Winkler et al.

2.3 Fluctuation-dissipation theorem

Similar to Onsager's proof of the reciprocal relations, this theorem is developed based on fluctuations in the system. We start by defining the total local fluxes for each of our fluids, $J_{i,tot}$, as the

sum of the local flux, J_i, and a random fluctuation, $J_{i,R}$. This gives us the following:

$$\begin{aligned} J_{w,tot} &= J_w + J_{w,R} \\ J_{n,tot} &= J_n + J_{n,R} \end{aligned} \tag{25}$$

Because the fluctuations $J_{i,R}$ are random, the following is true:

$$\langle J_{w,R} \rangle = \langle J_{n,R} \rangle = 0 \tag{26}$$

These fluctuations happen very rapidly, and on the microscopic, or molecular, scale. As such, their correlations have a very short range, and on the scale of our REV they are Gaussian white noise. Under these conditions, the fluctuation-dissipation theorem relates these fluctuations to the macroscopic properties of our system [12, 8, 4]. This relation has the following form:

$$\begin{aligned} \langle J_{w,R}(x,t) J_{w,R}((x'),(t')) \rangle &= 2k_B L_{ww} \delta(x-x') \delta(t-t') \\ \langle J_{n,R}(x,t) J_{n,R}((x'),(t')) \rangle &= 2k_B L_{nn} \delta(x-x') \delta(t-t') \\ \langle J_{w,R}(x,t) J_{n,R}((x'),(t')) \rangle &= 2k_B L_{wn} \delta(x-x') \delta(t-t') \\ \langle J_{n,R}(x,t) J_{w,R}((x'),(t')) \rangle &= 2k_B L_{nw} \delta(x-x') \delta(t-t') \end{aligned} \tag{27}$$

Here, the delta functions $\delta(x-x')$ and $\delta(t-t')$ are a result of the short ranged nature of these correlations, and have a value of one when integrated over all time/space. In our model, we will look at the flow through a slice of our system over time. We will use functions like those used by Winkler et al, which come from the same fluctuation-dissipation relationships. These are time correlation functions, C_{ij}, and are as follows:

$$\begin{aligned} C_{ww}(\tau) &= \langle \delta J_w(0) \delta J_w(\tau) \rangle \\ C_{nn}(\tau) &= \langle \delta J_n(0) \delta J_n(\tau) \rangle \\ C_{wn}(\tau) &= \langle \delta J_w(0) \delta J_n(\tau) \rangle \\ C_{nw}(\tau) &= \langle \delta J_n(0) \delta J_w(\tau) \rangle \end{aligned} \tag{28}$$

where $\langle \dots \rangle$ refers an expectation value, or ensemble average. Here, we define the fluctuations in our system as we did in equation (25), in terms of fluxes at time t, $J_i(t)$:

$$\begin{aligned} J_w(t) &= \langle J_w \rangle + \delta J_w(t) \\ J_n(t) &= \langle J_n \rangle + \delta J_n(t) \end{aligned} \tag{29}$$

where $\delta J_i(t)$ is the fluctuation from the average value. Rather than measuring the fluctuations directly, it is useful to rearrange our expression into terms measured by our simulator. We combine equations (28) and (29), and the derivation can be found in appendix E:

$$\begin{aligned} C_{ww}(\tau) &= \langle J_w(0) J_w(\tau) \rangle - \langle J_w \rangle \langle J_w \rangle \\ C_{nn}(\tau) &= \langle J_n(0) J_n(\tau) \rangle - \langle J_n \rangle \langle J_n \rangle \\ C_{wn}(\tau) &= \langle J_w(0) J_n(\tau) \rangle - \langle J_w \rangle \langle J_n \rangle \\ C_{nw}(\tau) &= \langle J_n(0) J_w(\tau) \rangle - \langle J_n \rangle \langle J_w \rangle \end{aligned} \tag{30}$$

By using the Green-Kubo method, we can compute the transport coefficients by integrating over all τ using the following:

$$L_{ij} = \int_0^\infty C_{ij}(\tau) d\tau \tag{31}$$

In our simulation, we measure flow rate, Q_i, of the wetting and non-wetting fluids rather than the mass flux. However, the flow rate is directly related to the flux by the following:

$$Q_i(t) = J_i(t)A_i(t) \tag{32}$$

where $A_i(t)$ is the wetting or non-wetting area of the slice. We can substitute these flow rates into the correlation functions to get:

$$\begin{aligned} C^Q_{ww}(\tau) &= \langle Q_w(0)Q_w(\tau)\rangle - \langle Q_w\rangle \langle Q_w\rangle \\ C^Q_{nn}(\tau) &= \langle Q_n(0)Q_n(\tau)\rangle - \langle Q_n\rangle \langle Q_n\rangle \\ C^Q_{wn}(\tau) &= \langle Q_w(0)Q_n(\tau)\rangle - \langle Q_w\rangle \langle Q_n\rangle \\ C^Q_{nw}(\tau) &= \langle Q_n(0)Q_w(\tau)\rangle - \langle Q_n\rangle \langle Q_w\rangle \end{aligned} \tag{33}$$

The integration changes form as well, to become:

$$\Lambda_{ij} = \int_0^\infty C^Q_{ij}(\tau)d\tau \tag{34}$$

where Λ_{ij} is the flow rate correlation coefficient. Our simulation collects the values at discrete time points, and as such we can sum over all values as a type of integration to determine Λ_{ij}. We will determine the self-correlated coefficients, Λ_{ww} and Λ_{nn}, as well as the cross-correlation coefficients, Λ_{wn} and Λ_{nw}, using the following equations:

$$\begin{aligned} \Lambda_{ww} &= \sum_{\tau=0} [\langle Q_w(0)Q_w(\tau)\rangle - \langle Q_w\rangle \langle Q_w\rangle] \\ \Lambda_{nn} &= \sum_{\tau=0} [\langle Q_n(0)Q_n(\tau)\rangle - \langle Q_n\rangle \langle Q_n\rangle] \\ \Lambda_{wn} &= \sum_{\tau=0} [\langle Q_w(0)Q_n(\tau)\rangle - \langle Q_w\rangle \langle Q_n\rangle] \\ \Lambda_{nw} &= \sum_{\tau=0} [\langle Q_n(0)Q_w(\tau)\rangle - \langle Q_n\rangle \langle Q_w\rangle] \end{aligned} \tag{35}$$

Symmetry of the cross-correlated flow rate coefficients implies symmetry of the cross-correlated conductivities. So, if the assumptions we made along the way are correct, and Onsager symmetry holds for this system, then we should see that $\Lambda_{ij} = \Lambda_{ji}$, and consequently $L_{ij} = L_{ji}$.

2.4 Lattice-Boltzmann model for two-phase flow

The *Lattice-Boltzmann model* [7], or *LBM*, is a mesoscopic model of the microscopic behaviour of interacting particles defined on a grid. It is an example of a *lattice gas model* [5], which is used for modelling gases and liquids in a wide range of systems. The idea is to simulate the behaviour of the system constituents at the mesoscopic level, and from there obtain the macroscopic behaviour via an averaging procedure over the lattice. More specifically, the *Navier-Stokes equations* [2, 24], or NSEs, are obtained in the continuum limit of the LBM via the *Chapman-Enskog expansion*, see section 2.6. This is in contrast to starting with conservation laws at the level of the NSEs, and from there refining to smaller scales.

In essence, implementation of lattice gas models consists of two central steps: propagation of particles, and collision of particles. The former happens at each time step in the simulation, and the latter is normally modelled in the same way, as happening at a single instance in time. In other words, there is no dependency on previous times when the collision is performed. The occupation number, i.e. how many particles there are of a certain particle, is tracked at each grid point as the

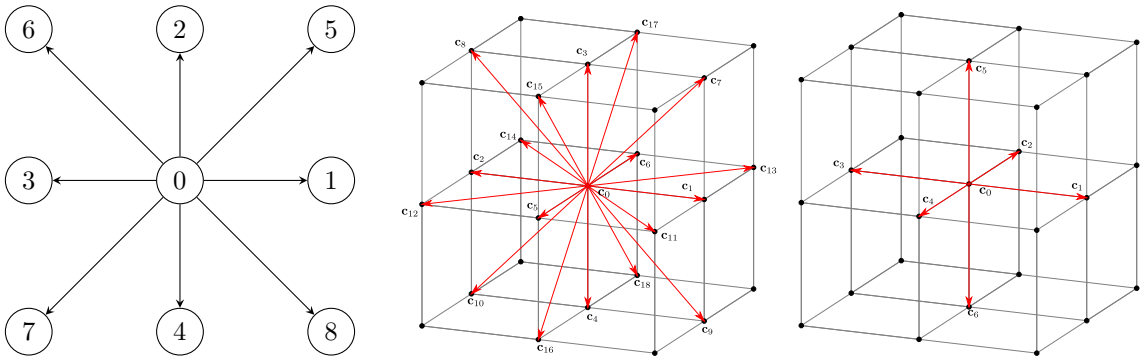

Figure 1: The lattice directions for a D2Q9-, D3Q19- and D3Q7-lattice.

components move and collide.

The lattice on which the particles move is specified in terms of a set of lattice vectors $\mathbf{c}_i$, where i numbers the possible directions of movement for the particle. The leftmost drawing in figure 1 shows a 2D example of such a lattice, with the lattice vectors labeled as $i = 0, 1, ..., 8$. The 0-direction is by convention the current lattice point itself, given by the vector $\mathbf{c}_0$. This lattice, with two dimensions and 9 lattice vectors, is called the *D2Q9-lattice*. In 3D, there can be more lattice directions, but the principle is the same, see figure 1. In the middle figure, there are 18 possible directions on the lattice at every point, and including the zero-vector of the current point, $\mathbf{c}_0 = \mathbf{0}$, we have 19 vectors in a 3D lattice. This gives us a *D3Q19-lattice*. Another common lattice which often is used to model the transport of bulk properties in 3D is the *D3Q7-lattice*. The lattice vectors here are simply the vectors pointing to the faces of the body-centered unit cell, giving a total of $6 + 1 = 7$ lattice vectors. In this project, the D3Q19-lattice is used for modelling momentum transport, and the D3Q7-lattice for mass transport of the two components.

After specifying a lattice by its lattice vectors $\mathbf{c}_i$, where i specifies the direction, one can calculate the evolution of the discrete local occupation number in the direction i, denoted n_i, of a species at a site $\mathbf{x}$ at a time t as

$$n_i(\mathbf{x} + \mathbf{c}_i, t + 1) \;=\; n_i(\mathbf{x}, t) + \Omega_i(\{n_i(\mathbf{x}, \mathbf{t})\}) \tag{36}$$

where $\mathbf{x} + \mathbf{c}_i$ is the position of a neighbouring lattice point and the time-step is set to 1. This jumping from lattice point to lattice point, or *streaming*, is linear, meaning that we can obtain the distributions at a lattice point from the neighbours on the lattice without considering a situation where the distributions interact while they move. The *collision operator* Ω gives the change in the occupation number n_i as an algebraic function of all n_i [5], a sum of terms which are products of different n_i. In short, at every lattice point, there is an individual number of particles n associated with each direction i at each lattice point. The key difference between lattice-gas models and the LBM is that in the latter, we use the mean particle population, or the *particle distribution*, instead of the discrete occupation number. To obtain this, we take the mean of equation (36), and apply the assumption that the occupation numbers n_i at a site are uncorrelated. This is the essence of the so-called *Boltzmann approximation*: the particles n_i do not interact with the particles $n_{i'}$, where $i' \neq i$. This entails that the collision process is completely local.

To obtain the LBM from the lattice-gas model above, we take the average of equation (36) and use the Boltzmann approximation. As a result, we can replace averages of products of the n_i, such as in the collision operator, with products of averages,

$$\langle n_i n_j \rangle \;= \langle n_i \rangle \langle n_j \rangle \;, \tag{37}$$

for two different occupation numbers i and j. For the averaged version of equation (36), we get an equation with the same form,

$$N_i(\mathbf{x}+\mathbf{c}_i, t+1) \;=\; N_i(\mathbf{x}, t) + \Omega_i(\{N_i(\mathbf{x}, \mathbf{t})\}) \;, \tag{38}$$

but with the discrete occupation numbers n_i replaced with the distribution N_i. For simple enough collision rules, where Ω can be expressed as a sum of products of the N_i, the collision of distributions can be performed in a single step, with only the requirement that Ω satisfies conservation of mass and momentum. The continuum limit of the LBM is built on the assumption that the lattice jumps are small compared to the scale of variation of the flow field $\mathbf{u}$ and density ρ, and on the existence of a *local equilibrium* for the distributions at each lattice point. This is used in the Chapman-Enskog procedure, see sec. 2.6, where the distribution N_i is split into an equilibrium N_i^{eq} and non-equilibrium N_i^{neq} part. The exact form of the equilibrium part depends on the lattice, and if we require lattice isotropy in addition to mass- and momentum-conservation. This is the case for the aforementioned D2Q9-, D3Q19- and D3Q7-lattices, and will be treated further in sec. 2.5 and in appendix A. The non-equilibrium part N_i^{neq} is assumed to be a linear function in the gradients of ρ and $\mathbf{u}$[5]. The local density and momentum is obtained in the single-component LBM by summing over the distributions at a lattice as

$$\rho\left(\mathbf{x}\right) \;=\; \sum_{i=0}^{Q-1} N_i\left(\mathbf{x}\right) \tag{39}$$

$$\mathbf{j} \;=\; \rho\mathbf{u} \;=\; \sum_{i=0}^{Q-1} N_i\left(\mathbf{x}\right)\mathbf{c}_i \tag{40}$$

$$\tag{41}$$

where Q is the number of lattice vectors in the lattice, e.g. 19 in the D3Q19-lattice. For this to be satisfied, we have from equation (38) that

$$\sum_i \Omega_i \;=\; \sum_i \Omega_i \mathbf{c}_i \;=\; 0 \;\; . \tag{42}$$

It is possible to consider other conservation laws in the LBM. For example, there exist LBM-formulations where thermodynamic free energy is used to determine the equilibrium distributions of the fluid species[5]. This makes it possible to satisfy conservation of total energy in the system, and is handled by an additional term in the equilibrium distribution. In addition to tracking the distributions of particle species as they propagate and collide on the lattice, one might also want to study the interaction with external forces and fields, such as the influence of pressure and temperature gradients, gravity and chemical reactions, to mention a few . These interactions are handled by introducing additional fields. However, this will not be considered in this project. The only additional field that will be introduced is a so-called *phase-field*, see sec. 2.5, which will determine the fluid phase in a region of the domain.

2.5 The Color-Lattice-Boltzmann model

There exist many different versions of the LBM depending on the type of system one wishes to examine. For incompressible two-phase flow in particular, one can use the so-called *Color Lattice-Boltzmann model* (CLBM) [15]. In the formulation of the model presented here, two equations defined on a D3Q7-lattice govern the mass transport for two immiscible components, in addition to one equation that governs the transport of momentum on a D3Q19-lattice. The “color” aspect

of the model means that this variant of LBM adds an interaction force between particle species which is linear in the density gradient, a so-called *phase indicator field* ϕ, defined as [1]

$$\phi\left(\mathbf{x}\right) = \frac{N_a - N_b}{N_a + N_b}\ , \tag{43}$$

where N_a and N_b are the number densities, also functions of $\mathbf{x}$, for fluid A and B respectively.

The phase field $\phi \in [-1, 1]$ is connected to the equilibrium contact angle between the fluid and solid as $\cos\theta_{\text{eq}} = \phi_{\text{eq}}$ for some stationary value ϕ_{eq} of the phase field $\phi(\mathbf{x})$. $\phi(\mathbf{x})$ gives us a way to calculate the interfacial tension via a mechanical definition. In a real system, and in LBPM, the interface between components is not sharply defined. Rather, it is diffuse over some length scale, which determines a volume between solid-fluid and fluid-fluid. In this interface-volume, the interfacial tension is not defined, since we don't have an exact dividing surface, often approximated as a *Gibbs surface*, on which we can construct the necessary tangential stresses to define a surface tension. In the CLBM, the Gibbs-surface is defined as where $\phi(\mathbf{x}) = 0$. In the solid, ϕ is assigned some constant value W, which will determine the wetting conditions of the system. In CLBM, the equilibrium interface profile can then be expressed as [15]

$$\Phi_A(\mathbf{x}) \ = \ \frac{1}{2\beta}\log\left(\frac{1+\phi(\mathbf{x})}{1-\phi(\mathbf{x})}\right) \tag{44}$$

where the label A means that $\Phi_A > 0$ in regions occupied by fluid A. β is a parameter that determines the thickness of the interface. Returning to the determination of the interfacial tension, we can integrate the normal and tangential stresses over the thickness of the interface between the solid and fluid (here fluid A) to get the fluid-solid interfacial tensions between the wall and fluid A and B, σ_{As} and σ_{Bs} respectively, as

$$\sigma_{As} \ = \ \int_{-\infty}^{x_s} \left(\sigma_{xx} - \sigma_{yy}\right) \mathrm{d}x \tag{45}$$

$$\sigma_{Bs} \ = \ \int_{x_s}^{\infty} \left(\sigma_{xx} - \sigma_{yy}\right) \mathrm{d}x \tag{46}$$

where x_s is the position of the solid wall, and σ_{xx} and σ_{yy} is the normal and tangential components of the stress tensor. The stresses and interface profile will deviate away from equilibrium, but the contact line in the CLBM can be shown to obey expected scaling behaviour when the interface is no longer stationary [13].

The transport of mass minimizes the diffusion of mass against the direction of a *color gradient*

$$\mathbf{C} = \nabla\phi \tag{47}$$

with normal vector $\mathbf{n} = \mathbf{C}/|\mathbf{C}|$. The equations for the mass transport are constructed such that it is favourable to minimize mass diffusion against the direction of $\mathbf{n}$. We will here be using the symbol $\mathbf{c}_i$ with index i to denote vectors on the D3Q19-lattice, and the notation $\mathbf{d}_q$ with index q to indicate D3Q7 lattice vectors. The two D3Q7 equations for the fluids labeled A and B are formulated as [16]

$$A_q(\mathbf{x}+\mathbf{d}_q, t+\delta t) = w_q N_a \left(1 + \frac{\mathbf{u}\cdot\mathbf{d}_q}{c_{s,D3Q7}^2} + \beta\frac{N_b}{N_a+N_b}\mathbf{n}\cdot\mathbf{d}_q\right) \tag{48}$$

$$B_q(\mathbf{x}+\mathbf{d}_q, t+\delta t) = w_q N_b \left(1 + \frac{\mathbf{u}\cdot\mathbf{d}_q}{c_{s,D3Q7}^2} - \beta\frac{N_a}{N_a+N_b}\mathbf{n}\cdot\mathbf{d}_q\right) \tag{49}$$

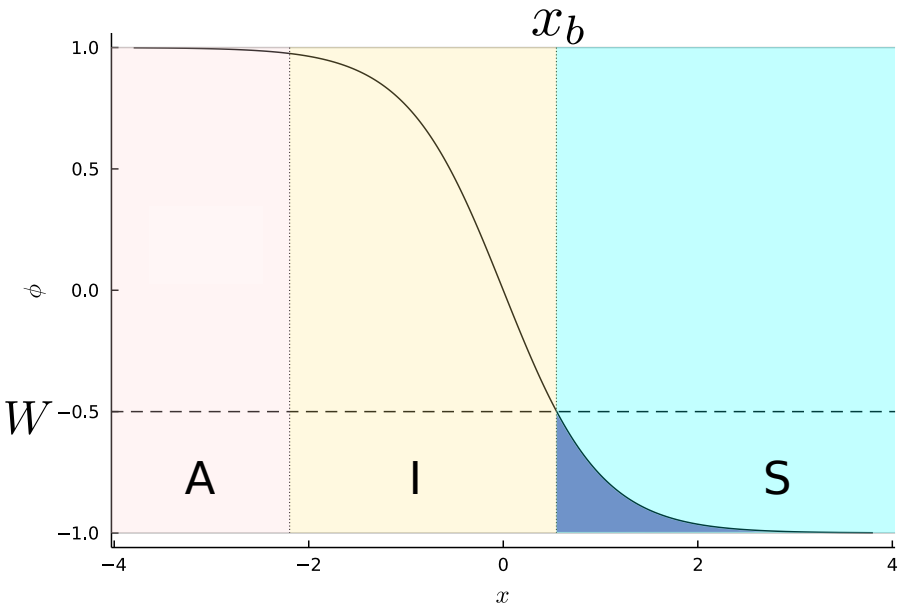

Figure 2: The interface region in the LBM, drawn in one dimension. A is one of the two fluid components, I is the interface region, and S is the solid wall. The assigned value of W determines the bounds of the integral that determines the fluid-solid interfacial tension. The dark blue area under the integral, within x_b, does not contribute to the interface tension.

where δt is some time step, $c_{s,D3Q7}$ is the speed of sound on the lattice, w_d is a set of weights determined by the lattice symmetry, and β controls the interface thickness. The component distributions ρ_A, ρ_B and momenta are calculated in the same way as in the single-component case (39), but summing over the distributions (48) and (49).

The equation that governs momentum transport is

$$N_i(\mathbf{x}+\mathbf{c}_i, t+\delta t) \;=\; N_i(\mathbf{x},t) + \sum_{k=0}^{18} M^{-1}_{i,k}\lambda_k(m^{eq}_k - m_k) + t_i\mathbf{c}_i \cdot \frac{\mathbf{F}}{c^2_{s,D319}}\;, \tag{50}$$

where $c^2_{s,D3Q19}$ is the speed of sound on the lattice, $\mathbf{F}$ is an external body force, and M^{-1}_{ik} is a matrix of coefficients which specifies the fluid-fluid interfacial tension [1]. The λ_ks is a set of relaxation times which determines how quickly the distributions relax to their equilibrium value, see appendix B. The distributions of different directions relax to equilibrium at different rates, which is often used in the description of porous media systems[15]. Such models with multiple relaxation times (MRT) is readily implemented on the D3Q7/D3Q19-lattices, and solves several problems inherent in single-time relaxation models [6].

m_k is a set of linear combinations of the form $\sum_{i=0}^{18} M_{ik}N_i(\mathbf{x},t)$, and the equilibrium moments m^{eq}_k specify the functional form of the interfacial tension, see appendix A. t_k are the symmetry weights corresponding to the D3Q19-lattice. Intuitively, the entire term containing the matrix $M_{i,k}$ can be thought of as the non-equilibrium contribution to the calculation of the new distribution $N_i(\mathbf{x}+\mathbf{c}_i, t+\delta t)$. The collision-operator Ω_i is in this case a function of the deviation from the equilibrium distribution, the fluctuation in the distribution at a specified time and position:

$$\Omega \;=\; \Omega(N_i(\mathbf{x}+\mathbf{c}_i,t) - N^{\text{eq}}_i(\mathbf{x}+\mathbf{c}_i,t))\;. \tag{51}$$

We refer to the appendix for the specific values of the above weights and coefficients, along with references for their derivation. We note that the fluid-fluid interfacial tension $\sigma_{ab} = 6\alpha$ follows from the calculation of the equilibrium moments. We also note that the equilibrium moments

corresponding to the density and fluid momentum are conserved [6].

The reference equilibrium density ρ_0 and kinematic viscosity ν are calculated as linear interpolations of the densities ρ_w, ρ_n and kinematic viscosities ν_w,ν_n of the individual fluids

$$\rho_0 = \frac{(1+\phi)\rho_n}{2} + \frac{(1-\phi)\rho_w}{2} \tag{52}$$

$$\nu = \frac{(1+\phi)\nu_n}{2} + \frac{(1-\phi)\nu_w}{2} \tag{53}$$

2.6 Navier-Stokes from LBM

The *Navier-Stokes equations*, or *NSEs*, describe the flow of gases and liquids in the continuum limit, i.e. when the flow can be described by smooth, continuous functions. They are obtained from the equations of motion of a general viscous, compressible *Newtonian fluid* [2, 24] by the additional assumptions that the fluid is isotropic (all directions are equivalent), the stress in the fluid is linear in the gradient of the fluid velocity, and that the divergence of the viscous stress for a fluid at rest is zero (meaning no sources of stress at rest). This situation is often called *incompressible* fluid flow, and allows us to obtain the NS-equations that describe an incompressible Newtonian fluid.

A strength of the LBM is that the NSEs are obtained in the continuum limit of an isotropic lattice, with the discrete populations of particles jumping on a lattice being replaced by continuous flow- and density-fields. The equations in this section will be stated for a single-component fluid, with the generalization to two fluids being treated elsewhere [3]. In the case of two-phase flow, the equations of motion for the fluids can, in the same way as for a single component, be obtained under appropriate conditions, see [1]. In the continuum limit, one will obtain the conventional form of the NSEs as in equation (56), but with extra surface-tension terms coupling the two fluids.

For a single-component fluid, the continuity equation reads

$$\frac{\partial \rho}{\partial t} + \nabla \cdot (\rho \mathbf{u}) = 0 \,, \tag{54}$$

where if we have *incompressible flow*, meaning that the density is constant within a small (infinitesimal in the continuum limit) volume following the flow, we have that $\partial\rho/\partial t = 0$. This implies that

$$\nabla \cdot \mathbf{u} = 0 \ . \tag{55}$$

With this additional constraint, the equations of motion for a compressible Newtonian fluid reduce to the NSE, which can be expressed as [7]

$$\rho \frac{\partial \mathbf{u}}{\partial t} + \rho(\nabla \cdot \mathbf{u})\mathbf{u} = -\nabla p + \mu \nabla^2 \mathbf{u} + \mathbf{F} \,, \tag{56}$$

where ∇p is a pressure gradient, and $\mathbf{F}$ is a body force such as gravity or a thermal gradient. If the spatial variations of the macroscopic variables ρ and $\mathbf{u}$ are considerably larger than the lattice spacing of the LB-model used, a steady state characterized by global mass- and momentum-transport is obtained as the system is propagated in time.

To actually obtain eq. (56) from eq. (38), one has to perform a Taylor expansion in both $\mathbf{x}$ and t, and keep terms up to second order in the so-called *Knudsen number* ϵ [5]. ϵ is defined as the ratio of the mean free path of the particles and the spatial scale of the variation L of the macroscopic variables ρ and $\mathbf{u}$. In the LBM, replacing the term 'particle' with 'distributions', the collision step

is applied at every lattice point, meaning that the mean free path of the particles is 1, if the lattice spacing is set to 1. If in addition the time step τ is set to 1, the particles move on the lattice at unit speed, meaning that the time to reach local equilibrium is of the order $\tau \sim 1$. We can then safely assume that the relaxation to global equilibrium is much larger than the time step τ. We then define the Knudsen number as

$$\epsilon = \frac{1}{L} . \tag{57}$$

The expansion itself which yields the NS equation (56) is not strictly relevant for this report, and will not be performed here. We refer to [5] for an outline of the procedure. Obtaining the equations of motion for the fluids including surface tension terms from the discretized LBM equations for mass-transport (48) and (49), and momentum transport (50) is also outside the scope of this report, and they will not be used here. We refer to [16] for the form of the equations of motions resulting from the above discretized transport equations, and to [10, 1] for their derivation.

2.7 Weak compressibility in LBM

Local equilibrium in LBMs is based on a second order expansion of the Maxwell distribution, and consequentially, this has implications for the validity of the model: the Mach number $\mathrm{Ma} = u/c_s$, where u and c_s are the typical lattice velocities and the speed of sound of the lattice, respectively, has to be reasonably small, typically $\mathrm{Ma} < 0.1 \sim 0.3$. It is only in this limit that the continuum equations for the fluid are valid. It follows from this that we are able to use LBMs even if the fluids involved are incompressible. The incompressibility condition $\nabla \cdot \mathbf{u} = 0$ pertains to the flow $\mathbf{u}$, and not the individual fluids, hence the choice $P = c_s^2 \rho$ as equation of state does not matter for small density variations. Even if this might look like a simple ideal-gas approximation, it does not mean that the interactions modelled by LBM are trivial. The strong molecular interactions between particles are simply restated as weak interactions between larger constituents, the fluid parcels at a more coarse-grained length scale. Strictly speaking, the LBM routine can handle incompressible fluids for density changes $\delta\rho/\rho$ on the order of $\sim \mathcal{O}(\mathrm{Ma}^2)$ [5]. We will be concerned with steady-state flow in this work, at flow velocities much smaller than the Mach number of the lattice, so the problem at hand is expected to be well within the limits of the LBM-procedure.

3 Method

To investigate whether Onsager reciprocity holds in two-phase flow in porous media, we will combine simulation using the Color Lattice-Boltzmann model with data analysis performed in `Julia`. The general outline of the method is as follows:

1. **Preparation of domain**
   (a) Select a domain, and generate a random fluid configuration at a specified saturation ($S_w = 0.25, 0.50, 0.75$).
   (b) Add inlet layers to minimize boundary effects.
   (c) Perform domain decomposition and assign fluid labels (solid, wetting, non-wetting) in the domain.
2. **Simulation step**
   (a) Determine input parameters of simulation from desired capillary and scaling quantity.
   (b) Run CLBM simulation on domain until steady-state is achieved, meaning a deviation in the capillary number within 1% over 10^4 time steps. Record the exact simulation state.
   (c) Restart the simulation from the point of steady state and collect data for a set amount of time.

3. **Analysis step**

   (a) Calculate the correlation function Λ_{ij} from the flow data Q_i, i =w,n output by the simulator.

The steps will be explained in the sections that follow. Before the individual steps are explained, we offer a brief explanation of how the simulator itself operates and what type of input is needed.

3.1 Simulation method and data

The simulations will be performed using a open source framework for one- and two-phase flow simulations, called *Lattice Boltzmann Methods for Porous Media* [16] (*LBPM* for short), a suite of simulation programs and protocols that utilizes different variants of the Lattice-Boltzmann model to obtain results on the macroscopic behaviour of fluids in different types of domains and systems. LBPM is part of the *Open Porous Media*-initiative, which encourages the mutual development and sharing of software pertaining to research on porous media.

LBPM is capable of performing simulations of two-phase flow in porous media via an implementation of the Color Lattice-Boltzmann model, see section 2.5. The routine can be run on an arbitrary domain, both user-specified or recreated samples of real porous material. In this project, a CT-scan of real porous materials was used as a simulation domain. All of the CT-data is available [19].

The CT-data consist of a series of 8-bit raw images organized in a array, in which we will identify the three dimensions with the (x, y, z)-axes. Each image is a CT-scan of a slice of the porous material, where the x- and y-coordinates denote the in-plane position. The z-coordinate specifies the direction perpendicular to each slice, the 'height'-coordinate in the sample. The coordinates are discrete, as the natural unit along the axes is the voxel length, the length of the side of the ≪pixel≫ which the image is made out of, which we will call a. The resolution, and therefore a, is determined by the CT-apparatus.

The simulator takes 8- or 16-bit images as input for the simulation domain. Each voxel in the simulation carries a label in the form of a 8-bit signed integer, which means it can take integer values in the range $[-127, 128]$. A label can determine for example which kind of fluid is located at that point, or if it is part of the solid matrix or wall. Negative labels (and 0) are taken to be immobile components in the domain, while positive is taken to be mobile. One can freely assign a *component affinity* $W \in [-1.0, 1.0]$ to each label, which determines the wetting condition for the immobile components. The wetting affinity W is connected to the equilibrium contact angle, see fig. 2. The two fluids in the simulation are labeled A and B, and the convention is such that a positive W makes A the wetting fluid (and vice versa).

The domain needs to be prepared before the CLB-simulation itself can be performed. This entails specifying the simulation domain to be used in the input image, specifying a processing grid (for parallel-processing over several CPUs/GPUs), boundary-conditions, setting the initial wetting saturation S_w for the sample, and choosing a routine of how the wetting fluid is initially distributed in the domain. In addition, a mixing layer can be added at one or both of the flow boundaries to account for the mismatch of pathways in the porous material when running simulations with periodic boundary conditions. Other adjustments can be done, but will not be relevant for the project at hand. The boundary conditions , initial S_w and its distribution are of particular interest. The boundary conditions can for example be periodic, or open with either constant volumetric flow-rate or pressure drop over the sample.

3.1.1 Preparation of domain

For the simulation domain, a CT-scan of a Bentheimer sandstone is used [19]. The resolution of the sample is 7μm, and the dimensions are $(x, y, z) = (601, 594, 1311)$ voxels. We use a subdomain from inside the sample of size $(300, 297, 500)$ voxels to perform the simulations on, as the region outside the sample itself is included in the image as solid voxels. The computational time is also more manageable for a smaller domain. The boundary conditions were periodic in the direction of overall flow $\sim z$. The simulation will be run in parallel on a pair of GPUs (NVIDIA Tesla P100 or Tesla V100), so the domain is segmented into two parts to be distributed over the GPUs.

20 random samples at a specified saturation were generated for each of the cases (in case B, 20 samples were generated for each saturation). We add a mixing layer of thickness 6 (voxels) at the inlet and outlet of the samples[16]. When considering a domain with periodic boundary consitions, the pores of the inlet and outlet don't necessarily match up, which leads to a blockage of the flow. By the inclusion of mixing layers, one is guaranteed to have no blockage of the flow pathways due to our definition of the boundary condition. The porosity is increased in the simulation-process, but the mixing layers are removed when the porosity is calculated in the end.

3.1.2 Simulation step

For the simulation step itself, we consider three different simulation cases with different sets of parameters.

A) $\sigma = 30$ mN/m , $\mu_w = \mu_n = 10^{-3}$ Pa·s, $W = 0$

B) $\sigma = 0$, $\mu_w = 5\mu_n = 10^{-3}$ Pa·s, $W = 0$

C) $\sigma = 30$ mN/m , $\mu_w = \mu_n = 10^{-3}$ Pa·s, $W = -0.5$

Here, σ is the interfacial surface tension, $\mu_i = \rho_i \nu_i$ is the dynamic viscosity of fluid i and is related to relaxation time τ_i in table 1, see appendix B, and W is the wetting affinity. Case A and B are similar to the ones considered in [25], but now done in a 3D model of a real porous material using the LB-model. Case A is chosen to obtain flow where the viscous dissipation of the two fluids are equal. Case B is an infinite capillary number case, chosen to represent a situation where the viscous forces dominate over the surface tension. We expand with a third case where we investigate the effect of wetting affinity on the walls. The simulation parameters for the three cases are summarized in table 1. The simulation parameters are all in dimensionless lattice units, and have to be related to physical values via rescaling, see appendix F.

		Case A	Case B	Case C
τ_A	Relaxation time of fluid A.	0.7	0.7	0.7
τ_B	Relaxation time of fluid B.	0.7	1.5	0.7
ρ_A	Density of fluid A in lattice units.	1.0	1.0	1.0
ρ_B	Density of fluid B in lattice units.	1.0	1.0	1.0
α	Surface tension parameter.	10^{-3}	0	10^{-3}
β	Interface width parameter.	0.95	0.95	0.95
F	External body force.	$3.36 \cdot 10^{-4}$	$3.36 \cdot 10^{-4}$	$3.36 \cdot 10^{-4}$
a	Voxel length.	7μm	7μm	7μm
(x, y, z)	System size in voxels.	$(300, 297, 500)$	$(300, 297, 500)$	$(300, 297, 500)$

Table 1: Values used in the LBPM simulation.

The criterion for steady state was calculated as in equation (59), with $\delta_s t = 20000$ and acceptance criterion $\Delta \mathrm{Ca}_a = 0.01$. We run all simulations with periodic boundary conditions and constant

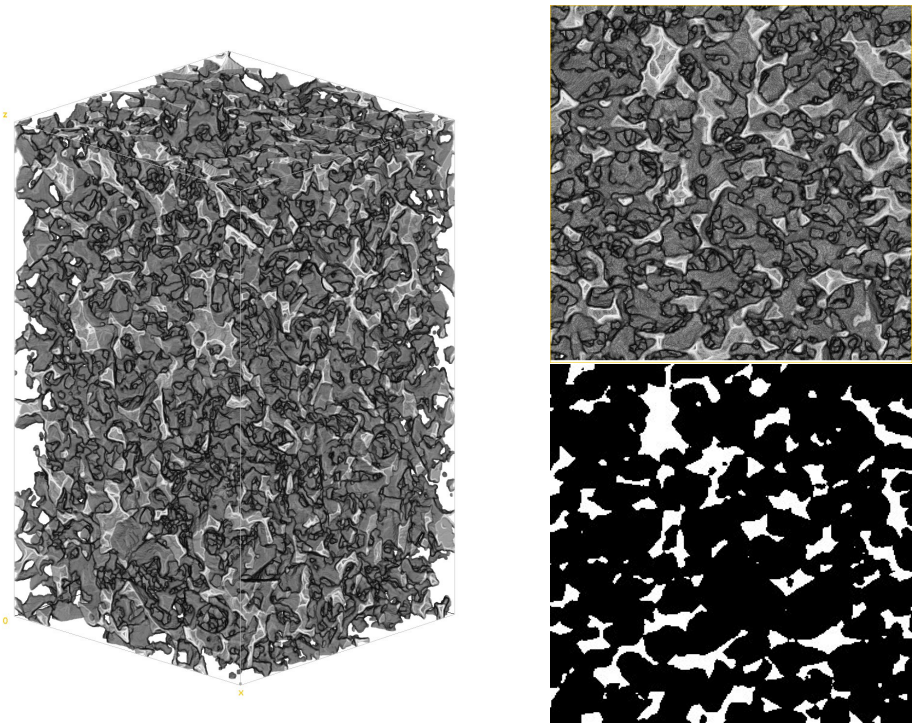

Figure 3: Left: 3D image of domain on which the simulation is run. Right: a slice in the xy-plane at $z = 250$, where the flow Q is measured, volume plot (above) and segmented image (below). The latter is what is seen by the simulator.

pressure drop $\Delta P/L = \Delta 100$ MPa/m over the domain to measure the fluctuations in Q_w and Q_n.

For this project in particular, the simulation domain was a Bentheimer sandstone, found under project number 172 on Digital Rocks Portal [19]. The CT-scan had a resolution of 7μm and $\phi \sim 0.19$. We simulated on a smaller subdomain of size $(300, 297, 500)$ voxels, with porosity $\phi \sim 0.182$. The simulation parameters were set as given in table 1. For case B), we ran simulations for the same wetting saturations to investigate the saturation-dependence of the auto- and cross-correlation coefficients. As in [25], we did this for $S_w = 0.25, 0.5, 0.75$.

The capillary number in the simulation is calculated as a sum of the individual capillary numbers of the fluids

$$\mathrm{Ca} \;=\; \frac{S_a \mu_a \mathbf{u}_a + S_b \mu_b \mathbf{u}_b}{\sigma_{ab}} \tag{58}$$

This definition gives a defined capillary number even if one of the fluids gets stuck and stops flowing. One often defines the capillary number in terms of one of the fluids as if there was single-phase flow. The exact value of Ca is not important, it is the magnitude that is important, so the fact that we use a different definition of Ca compared to[25] is not expected to matter. The CLB-routine uses the capillary number Ca to check for steady-state at a specified time-interval. The acceptance criterion for steady state is [16]

$$\Delta\mathrm{Ca} \;=\; \left| \frac{\mathrm{Ca}(t) - \mathrm{Ca}(t - \delta_s t)}{\mathrm{Ca}(t)} \right| \;<\; \Delta\mathrm{Ca}_a \quad , \tag{59}$$

where $\delta_s t$ is the time interval between each check for steady state and $\Delta\mathrm{Ca}_a$ is the user-set acceptance criterion. We use a relative tolerance of 0.01 in this work. Initial configurations were

generated randomly, meaning random wetting-voxels in the pore-space being inserted in the raw-data image of the domain until the desired saturation was reached. A natural extension would be to investigate the effect of the starting configuration on the final flow and correlation coefficients. However, for a high Ca steady state situation, the history-dependence of the system is expected to be very weak, as the random configurations quickly disappear.

After steady-state was achieved, the simulations were restarted and run for x time-steps. The flow rates Q_w and Q_n were measured through a slice in the xy-plane halfway through the sample, $z = 250$, see fig. 3. The porosity of the slice was approximately the same as that for the entire sample, $\phi_{\text{slice}} \sim 0.182$. We divide out the pore area from the flows Q_w, Q_n but we will continue to use the current notation. The flow rates were recorded at every 1000th time step, and we ran the simulation for 10^6 time steps.

3.1.3 Analysis step

After data gathering, the flow rates Q_w and Q_n were extracted from the output-files of the simulator. The ensemble average of the flows $\langle Q_i \rangle$ were calculated as the average flow rate of all the samples, done for every time-step. The results are averaged over the 20 simulation runs for the ensemble average $\langle \ldots \rangle$ in each of the cases. The integral in eq. 34 was then calculated from the data. The fluid velocities were also extracted from the simulation. All simulation parameters are in dimensionless lattice units. We give the results in the same lattice units, but the results can be rescaled to physical units using e.g. the viscosity or a physical value of the interfacial tension $\sigma_{ab,p}$, see sec. F. An interfacial tension of 30 mN/m was used to set the pressure drop in this work. Error estimation was done by computing the standard error for Λ_{ij} by calculating the integral 34 for each of the terms in the ensemble average individually.

3.2 REV construction

The transport-equations in this work are coarse-grained macroscopic quantities, as stated in section 2.2, and are defined as averages over a *Representative Elementary Volume* (REV), a homogeneous volume element of the medium representative of the system as a whole. In our case, the REV is as seen to the left in fig. 3. For a properly defined REV, the thermodynamic variables are extensive in the system size, as is expected in the macroscopic limit. A natural question is then how to determine what size this REV has, as a too big REV is not only computationally demanding to work with, but the fluctuations in the flow are washed out when the size of the REV becomes very large. If the REV is too small, one cannot discern a well-defined average from the fluctuations, and the measured quantities obtain a considerable dependence on the size of the system. We will not study the dependence on REV in this report and will only consider a single REV. Continued work on this point could follow the same lines as Winkler et al. [25]. The fluctuations are expected to be Gaussian with the inverse variance $1/\sigma^2$ being a function of the system volume V. One could take sizes of the REV and see if the inverse variance follows a relation $\sigma^{-2} \sim V$. Winkler et al. showed that the linear relation was more evident at low Ca and non-zero surface tension for a range of system sizes. In our 3D-case, the region of Ca, parameters and system sizes that yield additive, extensive thermodynamic quantities are not known, and would be a potential path to pursue in further work.

3.3 Results and discussion

In their studies of the 2D dynamic network model, Winkler et al. obtained negative cross-correlation coefficients [25]. They argued that this was expected in network flow; if one component on average advances faster, the other component has to move slower on average. This is the case in 2D, where the flow was measured through a 1D line transversal to the flow direction. In our case,

Table 2: Auto- and cross-correlation coefficients for the three cases to three significant digits, calculated for $S_w = 0.5$ and with $\Delta P = 100$ MPa/m. The coefficients are given in terms of lattice units. Uncertainty estimates are based on the standard error.

	Case A ($\sigma \neq 0$, $M = 1$, $W = 0$)	Case B ($\sigma = 0$, $M = 1/5$, $W = 0$)	Case C ($\sigma \neq 0$, $M = 1$, $W = -0.5$)
Λ_{ww} $[10^{-6}]$	110	44.5	132
Λ_{nn} $[10^{-6}]$	105	6.32	45.3
Λ_{wn} $[10^{-6}]$	104	19.3	78.4
Λ_{nw} $[10^{-6}]$	111	14.3	75.9
$\Lambda_{ww}\Lambda_{nn} - \Lambda_{wn}\Lambda_{nw}$ $[10^{-12}]$	35.1	3.01	37.8
($\delta\Lambda_{wn}$,$\delta\Lambda_{nw}$)	(0.253, 0.239)	(0.217, 0.282)	(0.269, 0.273)

Table 3: Auto- and cross-correlation coefficients for case B) to three significant digits, $\Delta P = 100$ MPa/m, for different saturations. Results are given in dimensionless lattice units.

	$S_w = 0.25$	$S_w = 0.50$	$S_w = 0.75$
Λ_{ww} $[10^{-6}]$	335	43.9	0.157
Λ_{nn} $[10^{-6}]$	0.0658	6.51	8.57
Λ_{wn} $[10^{-6}]$	5.52	19.7	1.65
Λ_{nw} $[10^{-6}]$	3.88	14.3	0.81
$\Lambda_{ww}\Lambda_{nn} - \Lambda_{wn}\Lambda_{nw}$ $[10^{-12}]$	0.64	3.01	0.00965

all cross-correlation coefficients are positive, which means that more flow of one of the components is correlated with a higher flow rate for the other fluid. A possible explanation for this difference is the dimensionality of the system. In a 3D porous material, the fluids have a lot more pathways to traverse through. An increase in the flow rate for one of the fluids does not necessarily mean that the other fluid is inhibited from moving, but rather that on average, both fluids are flowing faster if one increases in *this* slice in particular. Since the system is closed (periodic), the other component must, on average, move slower *somewhere* in the sample, but that could be in a slice which we are not observing.

By the second law of thermodynamics, we have that the auto-correlation coefficients in all of the cases should be positive. In addition, the inequality $\Lambda_{ww}\Lambda_{nn} - \Lambda_{wn}\Lambda_{nw} \geq 0$ should always hold if the system obeys Onsager symmetry, but the converse is not necessarily true. Of course, we don't know a priori if the system obeys this symmetry, but we note that the calculated inequalities in all of the cases are positive, along with the auto-correlations.

For case A ($\sigma \neq 0, M = 1, W = 0$), all of the coefficients are roughly equal. The fluids are equal in terms of viscous dissipation. There is no preference for either fluid at the walls of the medium, and hence, there is no mechanism that should be able to discern the fluids, and all of the coefficients are the same order of magnitude.

In case B, we have that Ca $\to \infty$, and it is for this case that we see the inequality $\Lambda_{ww}\Lambda_{nn} - \Lambda_{wn}\Lambda_{nw}$

Table 4: Darcy permeability (effective permeability of wetting- and non-wetting fluids) k_i output from simulator and permeability calculated from the flow as $Q_i/\Delta P$. The pressure used is the applied pressure drop in the simulation, and the values are calculated at $S_w = 0.5$. For the effective permeability from the simulator, a typical value was selected from the data.

	Case A	Case B	Case C
k_w and $Q_w/\Delta P$ $[10^{-6}]$	4.79 / 24.9	6.29 / 17.2	5.82 / 28.2
k_n and $Q_n/\Delta P$ $[10^{-6}]$	5.17 / 25.1	2.93 / 5.58	3.37 / 16.2

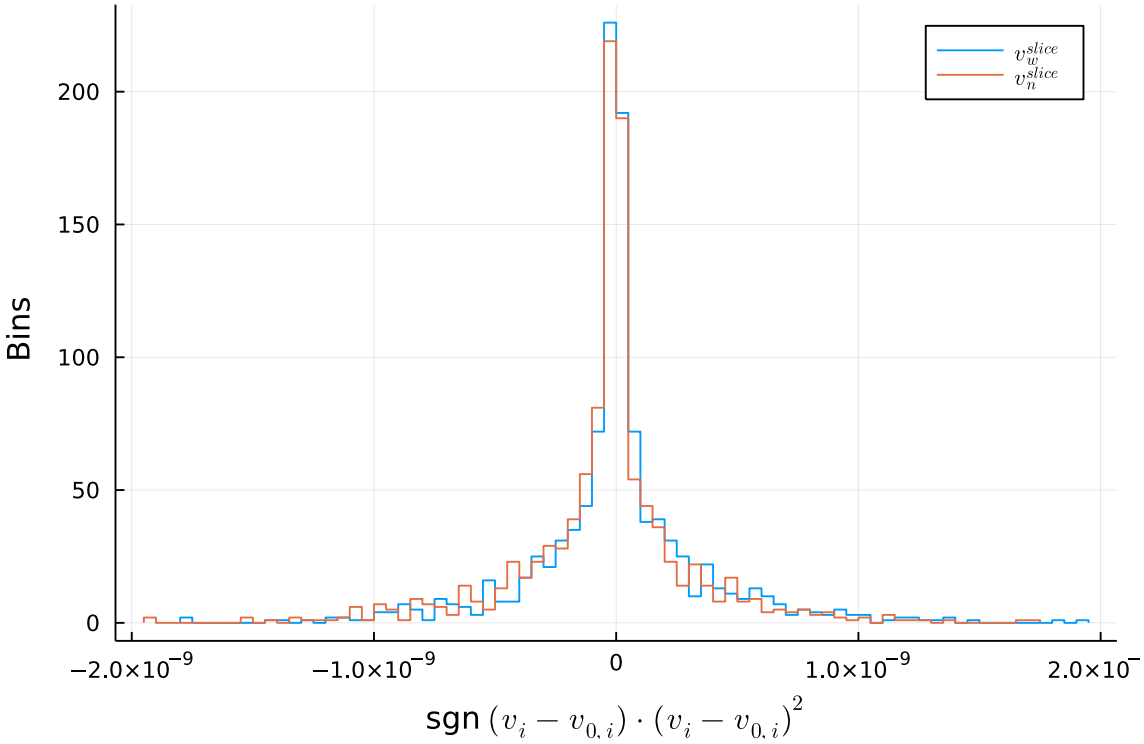

Figure 4: Fluid velocity of case A for the wetting- and non-wetting fluid, plotted for both fluids as $sgn(v - v_0) \cdot (v - v_0)^2$, with v_0 the average velocity. The histogram are plotted in lattice units.

closest to zero. This limit signifies linear dependence of the fluids [25], which lets us relate the auto-correlation coefficients to the cross-correlation coefficients by a relation $\Lambda_{ww} = \lambda^2 \Lambda_{nw}$. The constant λ is however saturation dependent and not close to the ratio of the viscosities, which is a departure from the findings on studies of the dynamic network model. The span of values in the coefficients is quite big depending on the saturation. The multi-relaxation CLBM has a more complicated dependence on the viscosities of the fluid, which determines the relaxation. Some of the relaxation times λ_k, which is determined by the viscosity ν alone, is as mentioned in appendix B possible to tune to geometry and for stability. The choice used in this work is a suitable choice for Stokes flow (small Reynolds number, large viscous forces, small length scales), but could have unpredictable effects on the transport coefficients, and requires further investigation.

For case C, the wetting affinity on the walls seems to alter the auto-correlation the most, but merely reducing the values of the cross-correlation coefficients compared to e.g. case A. A wetting affinity of -0.5 in the CLBM gives a moderate wetting, but for high enough capillary number the correlation between the fluids might not be affected in a substantial way since the advective inertial forces would be more important. However, in this regime the viscous dissipation increases, and if we have time-reversal invariance, we have the symmetry $\Lambda_{wn} = \Lambda_{nw}$. We see that the cross-correlation coefficients are still fairly equal in this case. This might indicate that the wetting properties of the wall does not have much to say for the symmetry of the cross-flow, with one possible reason being that the fluid that is "stuck" to the walls and contribute little to the bulk transport.

In all of the simulations, the interface thickness parameter β had a value of $\beta = 0.95$, which yields a sharp interface. Even with no surface tension, there exist passive interfaces between the fluids, and there is still a conversion between wetting- and nonwetting populations, as seen from the β-term in the mass transport equations (48) and (49). Here, the interface tension does not enter. The effect of zero interface thickness $\beta = 0$ is not investigated here, and its effects on the flow requires further study. At this point, it is unclear what effect the passive interfaces have on the coefficients, however, the β parameter is a factor in deciding what voxels LBPM deems part of the fluids or the interface. Voxels that are deemed part of the interface region are not considered part of the

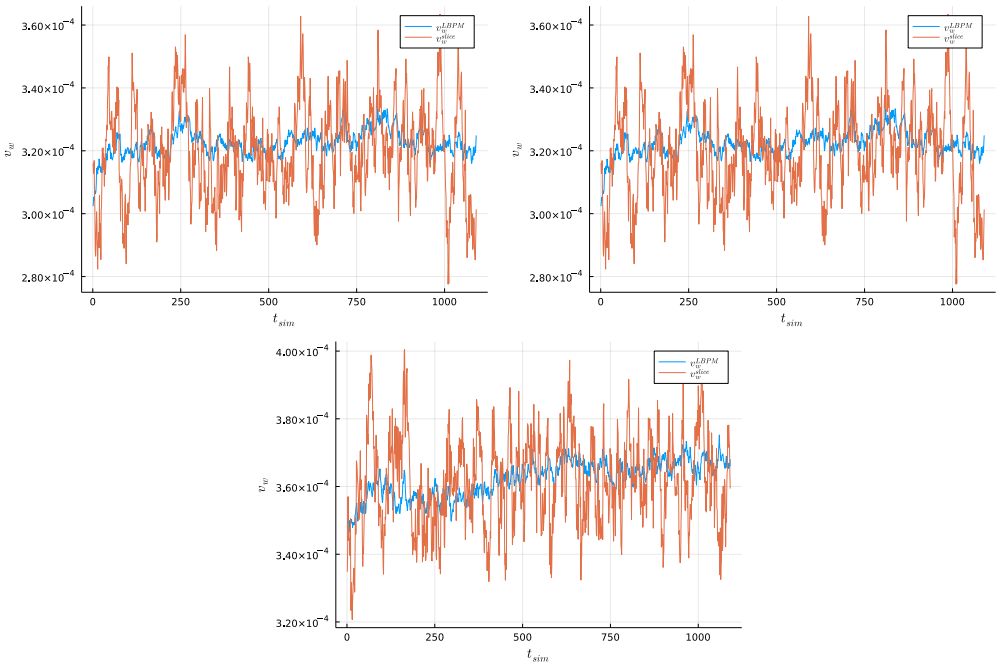

Figure 5: Wetting fluid velocities output from the simulator, indexed LBPM, and through the slice. The velocity reported by LBPM is the global average over all of the domain. Case A, B and C are plotted from left to right. The fluctuations through the slice are naturally larger than for the average velocity, but seems to be bounded and fluctuating around a well-defined mean.

flow of wetting- or non-wetting fluid in this work. If a large amount of voxels are counted as part of the interface, which depends on the densities, then this could affect the transport coefficients.

The time reversal invariance, which means $C_{ij}(\tau) = C_{ji}(\tau)$ in eq. 34, is a natural extension to the study. However, data was only gathered every thousand timestep in favour of collecting over long times. We can therefore not conclude on how the symmetry holds up for shorter times in this work. For large times, we only see the fluctuations around the mean flow, and the correlation function C_{wn} attains a well defined value for all times. The magnitude of the fluctuations for longer times, $\tau \geq 250000$, are of the order $\sim 5 - 10 \cdot 10^{-9}$. It is a bit unexpected that the correlation functions seems to attain different means for longer times. No matter the reason, it is evident that the case of infinite Ca might not have reached steady state at the point where we start to gather data. In future work, a stricter steady-state criterion has to be used, or the simulation could be run for a longer period of time before collecting data.

We apply the same pressure drop over the system as investigated in [25]. In case A and C, with finite capillary numbers, it is seen that the capillary number is a bit lower than in the 2D case of Winkler et al. The capillary number in our case is on the order of $\sim 2 \cdot 10^{-4}$, which is $10 - 20$ times smaller than in the dynamic network model studies of Winkler when applying the same pressure drop over the sample. This is an intermediate range of Ca, not quite in "high Ca"-regime, and applying a larger pressure drop over the sample might reveal different results. However, in general, there are many different variables that effects the results in this model applied to a complicated 3D-network, which makes it hard to isolate effects from each other, and future studies on the topic might wish to investigate simpler systems with the CLBM. The permeabilities in table 4 calculated from the data is three to four times smaller than what is given in table 2. The values output from the simulator is even smaller. This discrepancy was not treated further in this work, and a further investigation of this issue might double-check that we are actually computing the permeability in a sensible way (Q_i divided by the applied pressure drop) and with the units correct units, or into the effect of fluid connectivity.

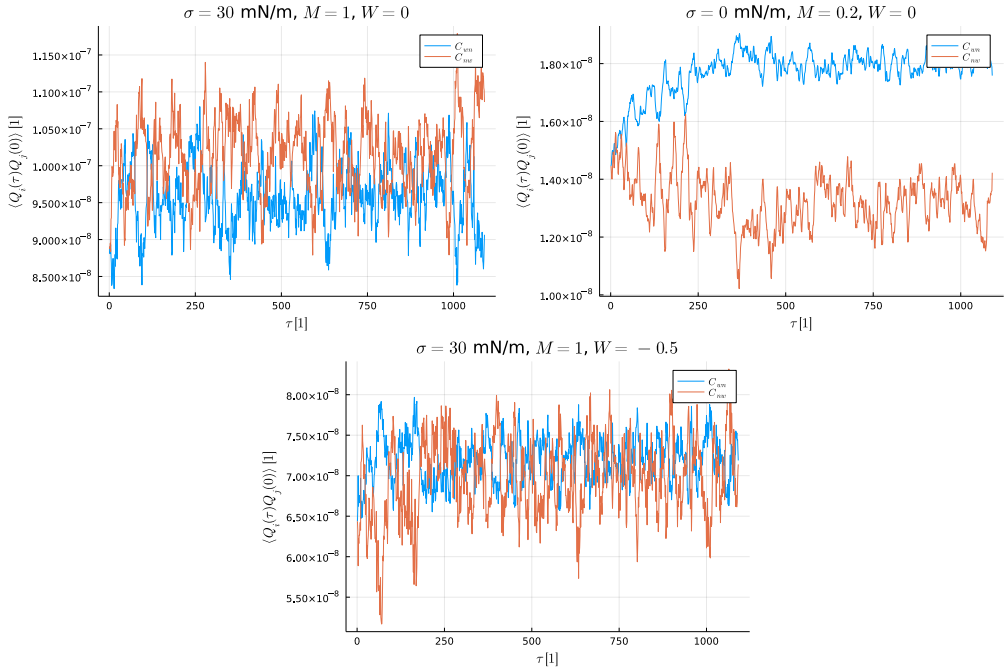

Figure 6: Cross-correlation functions for wetting- and non-wetting flow for all three cases. In the case with different viscosities, the correlation functions end up at different distinct mean values.

4 Conclusion

We have simulated two-phase flow in a CT-scan of a 3D porous material using a open source framework for the Color Lattice-Boltzmann model. Fluctuations around well-defined averages of the flow were obtained at steady-state, which we used to compute the auto- and cross-correlation coefficients of the flow using the Green-Kubo method under similar conditions as previous work using the dynamic network model. This yielded reasonable results in line with the second law of thermodynamics, with positive auto-correlation coefficients and positive semi-definite matrix Λ_{ij}. Approximately symmetric cross-coefficients was most apparent in the cases where the viscosity ratio was unity and surface tension was finite, but case B (unequal viscosities) was the closest to signifying linear dependence between the fluids, such as in previous work by Winkler et al. However, it seems that case B does not obey time-reversal symmetry for larger times, which might come from the multi-relaxation time scheme in the model, but this claim need further support and more thorough work. We know that the definition of steady state needs refinement in this case. The structure of the coefficients were expected for some of the cases (A,B), but more targeted studies are needed to find the effect of the different variables (viscosity, porosity, connectivity, Ca) have on the correlation functions. The question whether the phase field that determines the fluid phase has any effect on correlations is more comprehensive, and it might be more fruitful to study in a simpler system.

4.1 Further work

In potential future work, more care has to be taken to ensure that the case where Ca $\to \infty$ reaches steady state before data gathering. In addition, a study of the start-up of steady state with data-gathering at every time-step would be a way to further investigate the time-reversal symmetry. Due to time-constraints, a more thorough investigation of the permeabilities in table 4 was omitted, with the computed values for the Darcy permeability coming from hand-picked example values output by the simulator.

The effect of wetting on the auto- and cross-correlation coefficients are not clear, and would be a possible topic to explore. One would expect the symmetry of the cross-correlation to be broken

if the medium acquires a wetting affinity that favours one of the fluids, but we don't know how important this is for intermediate/high Ca. With a larger window of time and better access to computational resources, the number of samples could be increased to see if general results persist. One could make a more considerable effort in making sure the system has reached steady state by increasing the amount of time steps and decreasing the acceptance criterion for the capillary number. There is not a clear-cut answer for what causes the positivity of the cross-correlation coefficients, and the claim that it is due to the dimensionality of the system has to be investigated. A possible way to do this could be to study the topology of the porous material and vary e.g. the connectivity of the pathways to see if there exists a point where the cross-correlation coefficients flip sign. Comparison of flow in the dynamic network model in 3D would also be interesting to compare against.

Appendix

A The Collision Operator

We will in this appendix explain the form of the collision operator Ω in equation (38). We leave out the formal treatment of its derivation, and rather try to explain where it comes from. Including external forcing, expressed as

$$\Omega \;=\; \sum_{k=0}^{18} M^{-1}_{i,k}\lambda_k(m^{\mathrm{eq}}_k - m_k) + t_i\mathbf{c}_i\cdot\frac{\mathbf{F}}{c^2_{s,D319}}\;. \tag{60}$$

The expression above is often called the representation of the collision operator in the *moment basis*. The advection (lattice streaming) step is most easily performed in velocity-space, with direction given by e.g. the D3Q19 velocity set, while collision is more convenient to describe in collision-space, where the new basis-vectors are eigenvectors of the diagonal collision matrix λ_k [6], see appendix B. We denote this set of eigenvectors in collision space ξ_q.

One can construct these basis vectors in collision space as polynomials of the ones in velocity space by Gram-Schmidt orthogonalization [6]. The obtained basis elements has different ranks, resembling Hermite tensor polynomials [14]. To second order in space and first in time, the basis set consists of elements with symmetries corresponding to a scalar quantity, three components which together correspond to the momentum, and six components related to the stress tensor. Other moments correspond to higher order derivatives of the flow field, which does not occur in the incompressible NS-equations, and are subsequentially dropped [1]. This basis set is convenient when obtaining series solutions to the Boltzmann equation, and the second order elements of the basis results in surface tension-terms in the final NS-equations. The matrix M is a linear transformation between velocity space and moment space. The elements of the matrix M is defined in terms of the eigenvectors just mentioned. The moments $m_i = M_{i,k}f_k$ (with Einstein summation convention) are the distributions in velocity space represented in moment space, with the transformation given by the operator, or matrix, M. In essence, if the eigenvectors ξ_q are chosen such that they are eigenvectors of the diagonal matrix λ_k, the evolution of the distributions N_i in eq. (38) has the simple form[6]

$$N_i(\mathbf{x}+\mathbf{c}_i, t+1) - N_i(\mathbf{x},t) \;=\; -M^{-1}\hat{S}\left[m_i(\mathbf{x},t) - m^{\mathrm{eq}}_i(\mathbf{x},t)\right] \tag{61}$$

where the matrix $\hat{S}$ is a matrix with the relaxation rates along its diagonal. The left-hand side corresponds to the collision operator Ω_i. The moments m_i are divided into conserved and non-conserved, with their equilibrium value given by m^{eq}_i. For the conserved moments, we have $m_i = m^{\mathrm{eq}}_i$. The non-zero equilibrium moments m^{eq}_i can be obtained in the diagonalization procedure which leaves $\hat{S}$ diagonal. The one containing contributions from the surface tension have the form [1, 16]

$$\begin{aligned}
m^{\mathrm{eq}}_1 &= |\mathbf{j}|^2 - \alpha|\mathbf{C}| \\
m^{\mathrm{eq}}_9 &= \left(2j_x^2 - j_y^2 - j_z^2\right) + \alpha\frac{|\mathbf{C}|}{2}\left(2n_x^2 - n_y^2 - n_z^2\right) \\
m^{\mathrm{eq}}_{11} &= \left(j_y^2 - j_z^2\right) + \alpha\frac{|\mathbf{C}|}{2}\left(n_y^2 - n_z^2\right) \\
m^{\mathrm{eq}}_{13} &= j_xj_y + \alpha\frac{|\mathbf{C}|}{2}n_xn_y \\
m^{\mathrm{eq}}_{14} &= j_yj_y + \alpha\frac{|\mathbf{C}|}{2}n_yn_z \\
m^{\mathrm{eq}}_{15} &= j_xj_z + \alpha\frac{|\mathbf{C}|}{2}n_xn_z
\end{aligned}$$

where we have that the fluid-fluid interfacial tension σ_{ab} is related to the parameter *alpha* as $\sigma_{ab} = 6\alpha$. For athermal fluids, the conserved non-zero equilibrium moments are a scalar quantity $m_0^{\text{eq}} = \delta\rho$, corresponding to the mass density ρ, and three components $m_3^{\text{eq}} = \rho_0 u_x$, $m_5^{\text{eq}} = \rho_0 u_y$ and $m_7^{\text{eq}} = \rho_0 u_z$ that makes up a vector quantity corresponding to the momentum $\mathbf{j} = \rho\mathbf{u}$.

B Relaxation times

The relaxation times λ_k in equation (50) is given by

$$\lambda_k \;=\; \begin{cases} s_\nu, & k = 1,2,9,10,11,12,13,14,15 \\ \frac{8(2-\omega_\nu)}{8-\omega_\nu}, & k = 4,6,8,16,17,18,19 \end{cases}$$

where the relaxation parameter $\omega_{nu} = \tau^{-1}$, where the single relaxation-time parameter τ controls the kinmatic viscosity as $\nu = c_s^2(\tau - 0.5)$ [1]. The derivation of the matrix of relaxation parameters reveals that several of them are equal, and that some of them can be chosen in the range $[0, 2]$ (yielding linear stability), which the choice for $k = 4,6,8,16,17,18,19$ in eq. B is an example of. This choice can be used for tuning for a specific geometry, or for numerical performance[1].

C Onsager reciprocal relations

Combining equations (8) and (9) to produce the altered force term:

$$\begin{aligned} f(\alpha_1, \ldots, \alpha_n) &= \frac{e^{\Delta S/k_B}}{N_\alpha} \\ \ln f &= \ln e^{\Delta S/k_B} - \ln N_\alpha \\ \frac{\partial \ln f}{\partial \alpha_i} &= \frac{\partial}{\partial \alpha_i}\left(\frac{\Delta S}{k_B}\right) \\ \frac{\partial \ln f}{\partial \alpha_i} &= \frac{1}{k_B}\frac{\partial \Delta S}{\partial \alpha_i} \\ k_B \frac{\partial \ln f}{\partial \alpha_i} &= \frac{\partial \Delta S}{\partial \alpha_i} = \frac{k_B}{f}\frac{\partial f}{\partial \alpha_i} \\ X_i &= \frac{k_B}{f}\frac{\partial f}{\partial \alpha_i} \end{aligned} \tag{62}$$

Determining the ensemble average of the product $\alpha_i X_j$ using equation (12):

$$\begin{aligned} \langle \alpha_i X_j \rangle &= \int_{-\infty}^{\infty} d\alpha_i \ldots d\alpha_n \alpha_i X_i f(\alpha_i, \ldots, \alpha_n) \\ &= \int_{-\infty}^{\infty} d\alpha_i \ldots d\alpha_n \alpha_i \frac{k_B}{f}\frac{\partial f}{\partial \alpha_j} f \\ &= k_B \int_{-\infty}^{\infty} d\alpha_i \ldots d\alpha_n \alpha_i \frac{\partial f}{\partial \alpha_j} \\ &= -k_B \delta_{ij} \end{aligned} \tag{63}$$

D Entropy production

The derivation of the entropy production begins by substituting terms from the balance equations (16) into the local Gibbs equation (18):

$$\begin{aligned}\frac{\partial s}{\partial t} &= \frac{1}{T}\left(-\frac{\partial J_q}{\partial x}\right) - \frac{1}{T}\sum_{i=1}^{n}\mu_i\left(-\frac{\partial J_i}{\partial x}\right) \\ &= -\left(\frac{\partial}{\partial x}\frac{J_q}{T} - J_q\frac{\partial}{\partial x}\frac{1}{T}\right) + \sum_{i=1}^{n}\left(\frac{\partial}{\partial x}\frac{J_i\mu_i}{T} - J_i\frac{\partial}{\partial x}\frac{\mu_i}{T}\right) \\ &= -\frac{\partial}{\partial x}\frac{J_q}{T} + \sum_{i=1}^{n}\frac{\partial}{\partial x}\frac{J_i\mu_i}{T} + J_q\frac{\partial}{\partial x}\frac{1}{T} - \sum_{i=1}^{n}J_i\frac{\partial}{\partial x}\frac{\mu_i}{T}\end{aligned} \tag{64}$$

When we collect like terms we end up with the following equation:

$$\frac{\partial s}{\partial t} = -\frac{\partial}{\partial}\left(\frac{J_q}{T} - \sum_{i=1}^{n}\frac{J_i\mu_i}{T}\right) + J_q\frac{\partial}{\partial x}\frac{1}{T} - \sum_{i=1}^{n}J_i\frac{\partial}{\partial x}\frac{\mu_i}{T} \tag{65}$$

By comparing equation (65) to equation (17), we can determine the corresponding entropy flux:

$$J_s = \frac{J_q}{T} - \sum_{i=1}^{n}\frac{J_i\mu_i}{T} \tag{66}$$

and entropy production:

$$\sigma = J_q\frac{\partial}{\partial x}\frac{1}{T} - \sum_{i=1}^{n}J_i\frac{\partial}{\partial x}\frac{\mu_i}{T} \tag{67}$$

We would like to take J_q, which is not a measurable quantity, and instead express the entropy production in terms of the measurable heat flux, J_q. We use the following definition of J_q':

$$J_q' = J_q - \sum_{i=1}^{n}J_iH_i \tag{68}$$

Where H_i is the partial molar enthalpy of fluid i. In addition also need to use the definition of the chemical potential of fluid i at constant temperature, $d\mu_{i,T}$:

$$d\mu_{i,T} = d\mu_i + S_i dT \tag{69}$$

Where S_i is the partial molar entropy of fluid i. Then, by using equations (68) and (69), and

inserting them into equation (67), we obtain the following:

$$\begin{aligned}
\sigma &= J_q \frac{\partial}{\partial x}\frac{1}{T} - \sum_{i=1}^{n} J_i \frac{\partial}{\partial x}\frac{\mu_i}{T} \\
&= \left(J_q' + \sum_{i=1}^{n} J_i H_i\right)\frac{\partial}{\partial x}\frac{1}{T} - \sum_{i=1}^{n} J_i \left(\mu_i \frac{\partial}{\partial x}\frac{1}{T} + \frac{1}{T}\frac{\partial \mu_i}{\partial x}\right) \\
&= \left(J_q' + \sum_{i=1}^{n} J_i H_i\right)\frac{\partial}{\partial x}\frac{1}{T} - \sum_{i=1}^{n} J_i \left(\mu_i \frac{\partial}{\partial x}\frac{1}{T} + \frac{1}{T}\left(\frac{\partial \mu_{i,T}}{\partial x} - S_i \frac{\partial T}{\partial x}\right)\right) \\
&= \left(J_q' + \sum_{i=1}^{n} J_i H_i\right)\frac{\partial}{\partial x}\frac{1}{T} - \sum_{i=1}^{n} J_i \left(\mu_i \frac{\partial}{\partial x}\frac{1}{T} + \frac{1}{T}\left(\frac{\partial \mu_{i,T}}{\partial x} + S_i T^2 \frac{\partial}{\partial x}\frac{1}{T}\right)\right) \\
&= J_q' \frac{\partial}{\partial x}\frac{1}{T} - \sum_{i=1}^{n} J_i \frac{1}{T}\frac{\partial \mu_{i,T}}{\partial x} + \sum_{i=1}^{n} J_i H_i \frac{\partial}{\partial x}\frac{1}{T} - \sum_{i=1}^{n} J_i \left(\mu_i \frac{\partial}{\partial x}\frac{1}{T} + S_i T \frac{\partial}{\partial x}\frac{1}{T}\right) \\
&= J_q' \frac{\partial}{\partial x}\frac{1}{T} - \sum_{i=1}^{n} J_i \frac{1}{T}\frac{\partial \mu_{i,T}}{\partial x} + \sum_{i=1}^{n} J_i \left(H_i - \mu_i - S_i T\right)\frac{\partial}{\partial x}\frac{1}{T}
\end{aligned} \tag{70}$$

Since $H_i = \mu_i + S_i T$, then $H_i - \mu_i - S_i T = 0$ and the expression becomes:

$$\sigma = J_q' \frac{\partial}{\partial x}\frac{1}{T} + \sum_{i=1}^{n} J_i \left(-\frac{1}{T}\frac{\partial \mu_{i,T}}{\partial x}\right) \tag{71}$$

Now, for our system we have two fluids, one wetting and one non-wetting, and we can replace the generic J_i with the mass flux for our wetting, J_w, and non-wetting, J_n, fluids. By doing this we obtain the following:

$$\sigma = J_q' \frac{\partial}{\partial x}\frac{1}{T} + J_w \left(-\frac{1}{T}\frac{\partial \mu_{w,T}}{\partial x}\right) + J_n \left(-\frac{1}{T}\frac{\partial \mu_{n,T}}{\partial x}\right) \tag{72}$$

We would like for this expression to include terms for the volume of each fluid, V_i, and the pressure gradient, $\frac{\partial p}{\partial x}$, as these are readily measurable quantities. We can accomplish this by introducing the definition of chemical potential at constant temperature and pressure, μ_i^c:

$$\frac{\partial \mu_i^c}{\partial x} = \frac{\partial \mu_{i,T}}{\partial x} - V_i \frac{\partial p}{\partial x} \tag{73}$$

Equation (73) can be reorganized and inserted into equation (72) to give us:

$$\frac{\partial \mu_{i,T}}{\partial x} = \frac{\partial \mu_i^c}{\partial x} + V_i \frac{\partial p}{\partial x}$$

$$\sigma = J_q' \frac{\partial}{\partial x}\frac{1}{T} + J_w \left(-\frac{1}{T}\left(\frac{\partial \mu_w^c}{\partial x} + V_w \frac{\partial p}{\partial x}\right)\right) + J_n \left(-\frac{1}{T}\left(\frac{\partial \mu_n^c}{\partial x} + V_n \frac{\partial p}{\partial x}\right)\right) \tag{74}$$

Our particular system is athermal, such that the temperature gradient is 0 and the entropy production becomes:

$$\sigma = J_w \left(-\frac{1}{T}\left(\frac{\partial \mu_w^c}{\partial x} + V_w \frac{\partial p}{\partial x}\right)\right) + J_n \left(-\frac{1}{T}\left(\frac{\partial \mu_n^c}{\partial x} + V_n \frac{\partial p}{\partial x}\right)\right) \tag{75}$$

E Fluctuation-dissipation theorem

In order to obtain a time correlation function containing values measured by our simulator, rather than the fluctuations, we combine equations (28) and (29):

$$\begin{aligned}\langle \delta J_i(0)\delta J_j(\tau)\rangle &= \langle (J_i(0)-\langle J_i\rangle)\,(J_j(\tau)-\langle J_j\rangle)\rangle \\ &= \langle J_i(0)J_j(\tau) - J_i(0)\,\langle J_j\rangle - \langle J_i\rangle\, J_j(\tau) + \langle J_i\rangle\,\langle J_j\rangle\rangle\end{aligned} \tag{76}$$

Where $\langle J_i(0)\,\langle J_j\rangle\rangle$ and $\langle\langle J_i\rangle\, J_j(\tau)\rangle$ both become $\langle J_i\rangle\,\langle J_j\rangle$, and so we get the following:

$$\begin{aligned}\langle \delta J_i(0)\delta J_j(\tau)\rangle &= \langle J_i(0)J_j(\tau) - \langle J_i\rangle\,\langle J_j\rangle - \langle J_i\rangle\,\langle J_j\rangle + \langle J_i\rangle\,\langle J_j\rangle\rangle \\ &= J_i(0)J_j(\tau) - \langle J_i\rangle\,\langle J_j\rangle\end{aligned} \tag{77}$$

Substituting this into equation (28) gives:

$$\begin{aligned}C_{ww}(\tau) &= \langle J_w(0)J_w(\tau)\rangle - \langle J_w\rangle\,\langle J_w\rangle \\ C_{nn}(\tau) &= \langle J_n(0)J_n(\tau)\rangle - \langle J_n\rangle\,\langle J_n\rangle \\ C_{wn}(\tau) &= \langle J_w(0)J_n(\tau)\rangle - \langle J_w\rangle\,\langle J_n\rangle \\ C_{nw}(\tau) &= \langle J_n(0)J_w(\tau)\rangle - \langle J_n\rangle\,\langle J_w\rangle\end{aligned} \tag{78}$$

F Scaling and units in LBM

As the LBM is formulated on a discrete lattice, quantities in the model such as length, time, density viscosity etc. will be different from their physically observable counterparts. The connection between lattice-quantities and experiment is made by rescaling the lattice units to physical units. In LBPM, the timestep can be set in several ways, which again determines the length of processes that one can simulate. We will here use subscript p for physical quantities. The lattice quantities all have a unit 1, and have to be connected to experiment by rescaling. The fundamental physical units needed for rescaling are the time Δt_p (also called the *timestep*), the resolution (or length scale) a_p, and the mass unit m_p [20]. The length scale a_p is set from the resolution of the system, or in the case of LBM, the image reslution or voxel length. The mass unit m_p is set from the specific fluid used. The time scale can be determined from e.g. setting the physical kinematic viscosity ν_p or the interfacial tension $\sigma_{ab,p}$, which we can relate to the lattice units by dimensional analysis. We can then define the timestep Δt_p from this: dimensional analysis yields that the lattice value of the kinematic viscosity ν_l is scaled as $\nu_p = \nu\left(a_p^2/\Delta t_p\right)$, which can serve as a definition of Δt_p [21]

$$\Delta t_p \;=\; \left(\frac{\nu}{\nu_p}\right) a_p^2\,. \tag{79}$$

In the simulation, the fluid-fluid interfacial tension σ_{ab} is set via the dimensionless parameter α as $\sigma_{ab} = 6\alpha$. The physical interfacial tension $\sigma_{ab,p}$ and pressure P_p is obtained by scaling of the corresponding lattice quantities as

$$\sigma_{ab,p} = \sigma_{ab} m_p/\Delta t_p^2 \tag{80}$$

$$P_p = P m_p/(a_p \Delta t_p^2)\;\; . \tag{81}$$

One is free to choose which physical parameter to perform the rescaling with. One possibility is the interfacial tension: by choosing a representative value of this parameter, the rest of the numerical quantities can be scaled to physical ones. The physical mass m_p can via eq. 80 be expressed as $m_p = (\sigma_{ab,p}/\sigma_{ab})\left((\nu/\nu_p)\,a_p^2\right)^2$. From this, we get that the physical pressure P_p, can be expressed as $P_p = P\,(\sigma_{ab,p}/\sigma_{ab})\,a_p^{-1}$. Solving for P, we can use this to relate a physical pressure drop ΔP_p over a length L_z, the sample length in lattice units, to a simulated body force $\mathbf{F}$, which is used to

drive the flow.

As mentioned in sec. 2.5, the influence of a general body force $\mathbf{F}$ on all particles in the distribution function (50) is handled through the term $t_i \mathbf{c}_i \cdot \frac{\mathbf{F}}{c_{s,D319}^2}$. Applying a force in e.g. the z-direction, we have $\mathbf{c_i} \cdot \mathbf{F} = F_z$, the relevant weight is $t_5 = 1/18$ and $c_{s,D3Q19} = 1/\sqrt{3}$ as before. This is equivalent to specifying fixed inlet- and outlet pressures on the z-boundary, leading to a constant pressure drop $\Delta P/L$ over the domain.

References

[1] B. Ahrenholz et al. 'Prediction of Capillary Hysteresis in a Porous Material Using Lattice-Boltzmann Methods and Comparison to Experimental Data and a Morphological Pore Network Model'. In: *Advances in Water Resources*. Quantitative Links between Porous Media Structures and Flow Behavior across Scales 31.9 (Sept. 2008), pp. 1151–1173. ISSN: 0309-1708. DOI: 10.1016/j.advwatres.2008.03.009.

[2] G. K. Batchelor. *An Introduction to Fluid Dynamics*. Cambridge Mathematical Library. Cambridge: Cambridge University Press, 2000. ISBN: 978-0-521-66396-0. DOI: 10.1017/CBO9780511800955.

[3] T. Blesgen. 'A Generalization of the Navier-Stokes Equations to Two-Phase Flows'. In: *Journal of Physics D: Applied Physics* 32.10 (Jan. 1999), pp. 1119–1123. ISSN: 0022-3727. DOI: 10.1088/0022-3727/32/10/307.

[4] Herbert B. Callen and Theodore A. Welton. 'Irreversibility and Generalized Noise'. en. In: *Physical Review* 83.1 (July 1951), pp. 34–40. ISSN: 0031-899X. DOI: 10.1103/PhysRev.83.34. URL: https://link.aps.org/doi/10.1103/PhysRev.83.34 (visited on 14th Dec. 2021).

[5] Shiyi Chen and Gary D. Doolen. 'Lattice Boltzmann Method for Fluid Flows'. In: *Annual Review of Fluid Mechanics* 30.1 (1998), pp. 329–364. DOI: 10.1146/annurev.fluid.30.1.329.

[6] Dominique D'Humières et al. 'Multiple-Relaxation-Time Lattice Boltzmann Models in Three Dimensions'. In: *Philosophical transactions. Series A, Mathematical, physical, and engineering sciences* 360 (Apr. 2002), pp. 437–51. DOI: 10.1098/rsta.2001.0955.

[7] Jens Feder, Eirik Grude Flekkøy and Alex Hansen. *Physics of Flow In Porous Media*, p. 355.

[8] Melville S. Green. 'Markoff Random Processes and the Statistical Mechanics of Time-Dependent Phenomena. II. Irreversible Processes in Fluids'. en. In: *The Journal of Chemical Physics* 22.3 (Mar. 1954), pp. 398–413. ISSN: 0021-9606, 1089-7690. DOI: 10.1063/1.1740082. URL: http://aip.scitation.org/doi/10.1063/1.1740082 (visited on 14th Dec. 2021).

[9] Niklas Heinemann et al. 'Enabling large-scale hydrogen storage in porous media – the scientific challenges'. en. In: *Energy & Environmental Science* 14.2 (2021), pp. 853–864. ISSN: 1754-5692, 1754-5706. DOI: 10.1039/D0EE03536J. URL: http://xlink.rsc.org/?DOI=D0EE03536J (visited on 13th Dec. 2021).

[10] Dirk Kehrwald. 'Numerical Analysis of Immiscible Lattice BGK'. In: (2002).

[11] Signe Kjelstrup and Dick Bedeaux. *Non-equilibrium thermodynamics of heterogeneous systems*. Series on advances in statistical mechanics v. 16. OCLC: ocn191658618. Hackensack, NJ: World Scientific, 2008. ISBN: 9789812779137.

[12] R Kubo. 'The fluctuation-dissipation theorem'. In: *Reports on Progress in Physics* 29.1 (Jan. 1966), pp. 255–284. ISSN: 00344885. DOI: 10.1088/0034-4885/29/1/306. URL: https://iopscience.iop.org/article/10.1088/0034-4885/29/1/306 (visited on 13th Dec. 2021).

[13] M. Latva-Kokko and Daniel H. Rothman. 'Scaling of Dynamic Contact Angles in a Lattice-Boltzmann Model'. In: *Physical Review Letters* 98.25 (June 2007), p. 254503. DOI: 10.1103/PhysRevLett.98.254503.

[14] Parul Maheshwari, Gautam Mukhopadhyay and Siddhartha SenGupta. 'Properties of Tensor Hermite Polynomials'. In: *arXiv:1411.7398 [math-ph]* (Nov. 2014). arXiv: 1411.7398 [math-ph].

[15] J. E. McClure, J. F. Prins and C. T. Miller. 'A Novel Heterogeneous Algorithm to Simulate Multiphase Flow in Porous Media on Multicore CPU–GPU Systems'. en. In: *Computer Physics Communications* 185.7 (July 2014), pp. 1865–1874. ISSN: 0010-4655. DOI: 10.1016/j.cpc.2014.03.012.

[16] James E. McClure et al. 'The LBPM Software Package for Simulating Multiphase Flow on Digital Images of Porous Rocks'. In: *Computational Geosciences* (Jan. 2021). ISSN: 1573-1499. DOI: 10.1007/s10596-020-10028-9.

[17] Lars Onsager. 'Reciprocal Relations in Irreversible Processes. I.' en. In: *Physical Review* 37.4 (Feb. 1931), pp. 405–426. ISSN: 0031-899X. DOI: 10.1103/PhysRev.37.405. URL: https://link.aps.org/doi/10.1103/PhysRev.37.405 (visited on 14th Dec. 2021).

[18] Lars Onsager. 'Reciprocal Relations in Irreversible Processes. II.' en. In: *Physical Review* 38.12 (Dec. 1931), pp. 2265–2279. ISSN: 0031-899X. DOI: 10.1103/PhysRev.38.2265. URL: https://link.aps.org/doi/10.1103/PhysRev.38.2265 (visited on 14th Dec. 2021).

[19] Thomas Ramstad. *Bentheimer micro-CT with waterflood*. http://www.digitalrocksportal.org/projects/172. 2018. DOI: doi:10.17612/P7795W.

[20] Thomas Ramstad, Pål-Eric Øren and Stig Bakke. 'Simulation of Two-Phase Flow in Reservoir Rocks Using a Lattice Boltzmann Method'. In: *SPE Journal* 15.04 (July 2010), pp. 917–927. ISSN: 1086-055X. DOI: 10.2118/124617-PA.

[21] Marcel Schaap et al. 'Comparison of Pressure-Saturation Characteristics Derived from Computed Tomography and Lattice Boltzmann Simulations'. In: *Water Resources Research - WATER RESOUR RES* 431 (Dec. 2007). DOI: 10.1029/2006WR005730.

[22] Gurwinder Singh et al. 'Emerging trends in porous materials for CO $_2$ capture and conversion'. en. In: *Chemical Society Reviews* 49.13 (2020), pp. 4360–4404. ISSN: 0306-0012, 1460-4744. DOI: 10.1039/D0CS00075B. URL: http://xlink.rsc.org/?DOI=D0CS00075B (visited on 14th Dec. 2021).

[23] *THE 17 GOALS — Sustainable Development*. URL: https://sdgs.un.org/goals (visited on 13th Dec. 2021).

[24] Frank M. White. *Fluid Mechanics*. Nov. 2020.

[25] Mathias Winkler et al. 'Onsager-Symmetry Obeyed in Athermal Mesoscopic Systems: Two-Phase Flow in Porous Media'. In: *Frontiers in Physics* 8 (Apr. 2020), p. 60. ISSN: 2296-424X. DOI: 10.3389/fphy.2020.00060.